

# Galaxy And Mass Assembly (GAMA): the red fraction and radial distribution of satellite galaxies

Matthew Prescott,<sup>1\*</sup> I.K. Baldry,<sup>1</sup> P.A. James,<sup>1</sup> S.P. Bamford,<sup>2</sup> J. Bland-Hawthorn,<sup>3</sup> S. Brough,<sup>4</sup> M.J.I. Brown,<sup>5</sup> E. Cameron,<sup>6</sup> C.J. Conselice,<sup>2</sup> S.M. Croom,<sup>3</sup> S.P. Driver,<sup>7</sup> C.S. Frenk,<sup>8</sup> M. Gunawardhana,<sup>3</sup> D.T. Hill,<sup>7</sup> A.M. Hopkins,<sup>4</sup> D.H. Jones,<sup>4</sup> L.S. Kelvin,<sup>7</sup> K. Kuijken,<sup>9</sup> J. Liske,<sup>10</sup> J. Loveday,<sup>11</sup> R.C. Nichol,<sup>12</sup> P. Norberg,<sup>13</sup> H.R. Parkinson,<sup>13</sup> J.A. Peacock,<sup>13</sup> S. Phillipps,<sup>14</sup> K.A. Pimbblet,<sup>5</sup> C.C. Popescu,<sup>15</sup> A.S.G. Robotham,<sup>7</sup> R.G. Sharp,<sup>16</sup> W.J. Sutherland,<sup>17</sup> E.N. Taylor,<sup>3</sup> R.J. Tuffs,<sup>18</sup> E. van Kampen,<sup>10</sup> and D. Wijesinghe<sup>3</sup>

<sup>1</sup>*Astrophysics Research Institute, Liverpool John Moores University, Twelve Quays House, Egerton Wharf, Birkenhead, CH41 1LD, UK*

<sup>2</sup>*Centre for Astronomy and Particle Theory, University of Nottingham, University Park, Nottingham NG7 2RD, UK*

<sup>3</sup>*Sydney Institute for Astronomy, School of Physics, University of Sydney, NSW 2006, Australia*

<sup>4</sup>*Australian Astronomical Observatory, PO Box 296, Epping, NSW 1710, Australia*

<sup>5</sup>*School of Physics, Monash University, Clayton, Victoria 3800, Australia*

<sup>6</sup>*Department of Physics, Swiss Federal Institute of Technology (ETH-Zürich), 8093 Zürich, Switzerland*

<sup>7</sup>*School of Physics & Astronomy, University of St Andrews, North Haugh, St Andrews, KY16 9SS, UK*

<sup>8</sup>*Institute for Computational Cosmology, Department of Physics, Durham University, South Road, Durham DH1 3LE, UK*

<sup>9</sup>*Leiden University, P.O. Box 9500, 2300 RA Leiden, The Netherlands*

<sup>10</sup>*European Southern Observatory, Karl-Schwarzschild-Str. 2, 85748 Garching, Germany*

<sup>11</sup>*Astronomy Centre, University of Sussex, Falmer, Brighton BN1 9QH, UK*

<sup>12</sup>*Institute of Cosmology and Gravitation (ICG), University of Portsmouth, Dennis Sciamia Building, Burnaby Road, PO1 3FX, UK*

<sup>13</sup>*Institute for Astronomy, University of Edinburgh, Royal Observatory, Blackford Hill, Edinburgh EH9 3HJ, UK*

<sup>14</sup>*Astrophysics Group, HH Wills Physics Laboratory, University of Bristol, Tyndall Avenue, Bristol BS8 1TL*

<sup>15</sup>*Jeremiah Horrocks Institute, University of Central Lancashire, Preston PR1 2HE, UK*

<sup>16</sup>*Research School of Astronomy & Astrophysics Mount Stromlo Observatory Cotter Road Weston Creek, ACT 2611 Australia*

<sup>17</sup>*Astronomy Unit, Queen Mary University London, Mile End Rd, London E1 4NS, UK*

<sup>18</sup>*Max Planck Institute for Nuclear Physics (MPIK), Saupfercheckweg 1, 69117 Heidelberg, Germany*

Accepted 2011 June by MNRAS; received in original form 2011 January

## ABSTRACT

We investigate the properties of satellite galaxies that surround isolated hosts within the redshift range  $0.01 < z < 0.15$ , using data taken as part of the Galaxy And Mass Assembly survey. Making use of isolation and satellite criteria that take into account stellar mass estimates, we find 3514 isolated galaxies of which 1426 host a total of 2998 satellites. Separating the red and blue populations of satellites and hosts, using colour-mass diagrams, we investigate the radial distribution of satellite galaxies and determine how the red fraction of satellites varies as a function of satellite mass, host mass and the projected distance from their host. Comparing the red fraction of satellites to a control sample of small neighbours at greater projected radii, we show that the increase in red fraction is primarily a function of host mass. The satellite red fraction is about 0.2 higher than the control sample for hosts with  $11.0 < \log_{10} \mathcal{M}_* < 11.5$ , while the red fractions show no difference for hosts with  $10.0 < \log_{10} \mathcal{M}_* < 10.5$ . For the satellites of more massive hosts the red fraction also increases as a function of decreasing projected distance. Our results suggest that the likely main mechanism for the quenching of star formation in satellites hosted by isolated galaxies is strangulation.

**Key words:** surveys – galaxies: star formation – galaxies: interaction – galaxies: evolution – galaxies: formation – galaxies: dwarf.

## 1 INTRODUCTION

In recent years satellite galaxies have received much attention in both observational and theoretical studies in order to establish their role in the formation and evolution of galaxies. In the current  $\Lambda$ CDM models of the Universe, galaxies are assembled in a hierarchical fashion, whereby small halos of dark matter (DM) merge to form larger halos, in which baryonic matter then cools and condenses to form stars. In this framework satellite galaxies are associated with sub-halos of dark matter residing within the virial radii of larger halos, which are believed to be left over from an earlier assembly phase of their host. Thus the measurement of the spatial distribution of satellites, both in terms of their angular and radial distributions, can provide an insight into the mass accretion histories of galaxies.

The most common way to determine the radial distribution is to calculate the projected density of satellites surrounding samples of more luminous hosts, which requires redshifts and photometry of satellites and hosts. Previous studies which attempted to constrain the small-scale galaxy correlation function (Lake & Tremaine 1980; Phillipps & Shanks 1987; Vader & Sandage 1991; Lorrimer et al. 1994) or investigated the companions of field ellipticals (Madore et al. 2004; Smith et al. 2004) found that the projected density of satellites, as a function of radius, has a profile that can be described as a power law of the form  $\Sigma(R) \propto R^\alpha$ , with a slope,  $\alpha$  ranging between  $-0.5$  and  $-1.25$ . Subsequently, more accurate measurements of the projected density have been made, making use of larger and more complete redshift surveys, such as the 2-degree Field Galaxy Redshift Survey (2dFGRS, Colless et al. 2001) and the Sloan Digital Sky Survey (SDSS, York et al. 2000), allowing the production of large statistical samples of satellites and hosts selected using various well defined criteria (Sales & Lambas 2004; Chen et al. 2006; Ann et al. 2008; Chen 2008; Bailin et al. 2008).

Studies which have examined the radial distribution of satellites as a function of host luminosity, colour or morphology, have obtained mixed results. The first to divide their sample into early and late types was Lorrimer et al. (1994), who found the projected density profile of the satellites of early-type hosts to have steeper slopes and therefore to be more centrally concentrated than the satellites of late-type hosts. In contrast to this, Sales & Lambas (2005) using data from 2dFGRS, found that the distribution of the satellites of red hosts has a shallower profile than the satellites of blue hosts, which even deviates from a power law, flattening at small projected separation. More recently Chen (2008) using SDSS data, found that the satellites of both red and blue hosts follow similar power slopes after correcting for interlopers (galaxies mistaken as satellites through projection but not actually physically bound to their host).

Dividing their satellite sample into red and blue populations, Chen (2008) also finds that red satellites are more centrally concentrated than blue satellites, a trend which is also seen in the semi-analytic galaxy samples produced by Sales et al. (2007) using the Millennium Simulation. One explanation of this is that red satellites were accreted into their host's halo at earlier times than the blue satellites, which is consistent with the observational finding that red satellites have an anisotropic angular distri-

bution with a preference of being aligned along the major axes of their hosts (Brainerd 2005; Yang et al. 2006; Azzaro et al. 2007; Bailin et al. 2008; Agustsson & Brainerd 2010). Comparisons between the radial distribution of satellites and the dark matter distribution produced from simulations have also been conducted by Chen et al. (2006) and van den Bosch et al. (2005), who find that satellites are more centrally concentrated than dark matter sub-halos, but consistent with the dark matter profile.

Satellite galaxies not only provide useful information about the formation of galaxies but also about the processes that govern galaxy evolution in localised environments on scales of  $\sim 1$  Mpc. In the current theory of galaxy evolution it is thought that virtually all galaxies start off as blue, late-type discs which are then transformed by various processes into red, early types. This is supported by the observed bimodality of galaxies which can be seen out to  $z \sim 1$  (Bell et al. 2004; Willmer et al. 2006; Prescott et al. 2009), and studies such as Willmer et al. (2006) and Faber et al. (2007) which have shown there has been a doubling in the stellar mass density of galaxies on the red sequence over the last 7-8 Gyr.

The main processes believed to be responsible for transforming blue/late-type galaxies into red/early types involve the quenching of star formation, and include major-mergers (Toomre & Toomre 1972; Hopkins et al. 2008a), feedback from active galactic nuclei (Bower et al. 2006; Croton et al. 2006) and the depletion of gas reservoirs that fuel star formation. For satellite galaxies, the dominant process is most likely to be gas depletion, caused by the stripping of gas via a number of different hydrodynamical and radiative interactions with their hosts, acting over different timescales.

When a satellite halo is accreted by the larger halo of its host, hot gas from the satellite may be removed in the process known as strangulation (Larson et al. 1980; Balogh et al. 2000), resulting in the gradual decline in star formation over long timescales ( $> 1$  Gyr), as its fuel for future star formation is depleted. Star formation can be shut off more rapidly if the satellite is subjected to sufficient external pressure that its cold gas reservoir is removed in the process of ram-pressure stripping (Gunn & Gott 1972). Gas stripping via harassment (Moore et al. 1996) whereby the dark matter sub-halos of satellites are heated after undergoing frequent high-velocity encounters with other dark matter halos, is also a possibility, although this process is more likely to occur in galaxy clusters rather than small groups.

Recent studies using the SDSS have indicated that strangulation is the main mechanism causing the transition of satellites from the blue to the red sequence. Producing a group catalogue from DR2, Weinmann et al. (2006) investigate how the fractions of early- and late-type satellites vary as a function of halocentric radius, halo mass and luminosity, observing that the early-type fraction increases with decreasing halocentric radius, increasing halo mass and increasing luminosity. They argue that the increase in early-type fraction with luminosity at fixed halo mass is not expected if ram-pressure stripping or harassment is the primary cause of gas removal. Ann et al. (2008) use SDSS DR5 to investigate how the early-type fractions of satellites surrounding isolated hosts vary as a function of luminosity and projected distance. They find that the early-type satellite fraction increases significantly with decreasing projected ra-

dius for early-type hosts and stays approximately constant for late types. They conclude that hot X-ray emitting gas of the early-type hosts is responsible for the removal of gas.

Using an SDSS DR4 group catalogue, van den Bosch et al. (2008) compare the concentrations and colours of centrals and satellites of the same mass. By matching central and satellite pairs in both stellar mass and concentration, they find there is a significant difference in colour. Centrals and satellites matched in both stellar mass and colour, on the other hand, show no difference in concentration. Under the assumption that centrals are the progenitors of satellites (centrals change into satellites after being accreted into a larger halo), this implies that either the strangulation or ram pressure stripping process is occurring rather than harassment, which is believed to have a significant effect on the morphology of galaxies. Investigating the red fraction of satellites by mass they estimate that 70 per cent of satellite galaxies with  $\mathcal{M}_* = 10^9 \mathcal{M}_\odot$  have undergone satellite quenching in order to be on the red sequence at the present, with 30 per cent already red before becoming a satellite. For more massive satellites they find quenching to be less effective, with 65 per cent of satellites with  $\mathcal{M}_* = 10^{10} \mathcal{M}_\odot$  being red before accretion and virtually all satellites with  $\mathcal{M}_* = 10^{11} \mathcal{M}_\odot$  already being red before becoming satellites.

Furthermore, satellites are believed to affect the evolution of their hosts. Minor mergers between dwarf satellites and their central hosts provide one way in which to distort and thicken galaxy discs (Quinn et al. 1993) and enlarge the bulge components of discs (Domínguez-Palmero & Balcells 2008), and mergers involving gas-rich satellites may also provide gas which could prolong or replenish star formation in early-type spirals (White & Frenk 1991; Hau et al. 2008).

Finally, satellite systems analogous to the Milky Way (MW)-Magellanic clouds systems have also become of much interest lately due to their apparent rarity. Observational studies such as James & Ivory (2011), Liu et al. (2011) and Tollerud et al. (2011) find that only  $\sim 10$  per cent of MW like hosts have one Magellanic cloud like satellite and only  $\sim 5$  per cent have two. Similarly N-body simulations have shown that less than 10 per cent of MW sized dark matter haloes contain two Magellanic cloud sized sub-halos (Busha et al. 2010; Boylan-Kolchin et al. 2010).

In this paper we use data taken from the Galaxy And Mass Assembly (GAMA) survey to investigate: firstly the radial distribution of satellites surrounding a sample of isolated host galaxies, as a function of host mass and colour; and secondly how the red fraction of satellites depends on the projected distance between satellite and host, the stellar mass of the satellite and the stellar mass of the host. The GAMA redshift survey extends up to 2 mag deeper than the SDSS Main Galaxy Sample and, unlike previous studies, we use isolation criteria that take account of stellar mass estimates. The results are discussed in terms of the quenching mechanisms that act on satellites.

The structure of this paper is as follows. In Section 2 we outline the GAMA survey from which our samples of galaxies are taken. In Section 3 we define our criteria used to select isolated hosts and satellite galaxies. We also define how we select a control sample of neighbours. Section 4 describes how we divide the red and blue populations of galaxies, compare properties of the hosts and satellites, and determine the

projected density of satellites as a function of host mass and host colour. We show how the red fraction of satellites depends on satellite mass, host mass and projected radius and discuss potential processes that could produce these results in Section 5. Finally in Section 6 we summarise our main results. Throughout this paper we assume values of  $H_0 = 70 \text{ km s}^{-1} \text{ Mpc}^{-1}$ ,  $\Omega_m = 0.3$  and  $\Omega_\Lambda = 0.7$ .

## 2 DATA

### 2.1 Galaxy And Matter Assembly

GAMA is a project to construct a multi-wavelength (far-UV to radio) database of  $\sim 375\,000$  galaxies, by combining photometry and spectroscopy from the latest wide-field survey facilities (Driver et al. 2009, 2011). Currently covering  $144 \text{ deg}^2$  and going out to  $z \sim 0.5$ , GAMA will allow the study of galaxies and cosmology on scales between 1 kpc and 1 Mpc and provide the link between wide-shallow surveys, such as the SDSS Main Galaxy Sample (Strauss et al. 2002), 2dFGRS (Colless et al. 2001) and 6dFGRS (Jones et al. 2004), and narrow-deep surveys DEEP2 (Davis et al. 2003) and VVDS (Le Fèvre et al. 2005).

Central to GAMA is a redshift survey conducted at the 3.9-m Anglo-Australian Telescope (AAT) using the AAOmega spectrograph (Sharp et al. 2006), which is crucial to addressing the main objectives of the project. These include determining the dark matter halo mass function of groups and clusters (Eke et al. 2006), measuring the stellar mass function (Baldry et al. 2008) of galaxies down to Magellanic Cloud masses and determining the recent galaxy merger rate (De Propris et al. 2005).

The redshifts used in this paper were obtained as part of the initial spectroscopic survey known as GAMA I, carried out over 66 nights between March 2008 and May 2010. This consists of three  $12 \times 4 \text{ deg}$  fields at 9h, 12h and 14.5h (G09, G12 and G15) along the celestial equator and covering in total  $144 \text{ deg}^2$ . For detailed descriptions of the spectroscopic target selection and the tiling strategy used for GAMA, the reader is referred to Baldry et al. (2010) and Robotham et al. (2010), respectively. In brief, galaxies are selected for spectroscopy using an input catalogue drawn from the Sloan Digital Sky Survey (SDSS) Data Release 6 (Adelman-McCarthy et al. 2008) and UKIRT Infrared Deep Sky Survey (UKIDSS) (Lawrence et al. 2007).

In the following analysis we use data for galaxies which make up the *r*-band limited Main Survey, which contains in total 114 441 galaxies, which are spectroscopically selected to have Galactic extinction corrected Petrosian magnitudes (Petrosian 1976) of  $r_{\text{Petro}} < 19.4$  in fields G09 and G15 and  $r_{\text{Petro}} < 19.8$  in G12.

The high density of spectra per square degree of sky and high completeness of the redshift survey (98 per cent down to  $r_{\text{Petro}} = 19.8$ , Driver et al. 2011) required to achieve the main objectives of the project, make GAMA an ideal dataset to study satellite galaxies, since it does not suffer from the same incompleteness as other spectroscopic surveys due to fibre collisions. The SDSS for example has a minimum fiber spacing of 55 arcsec, resulting in 10 per cent of SDSS targets being missed from the spectroscopic sample because each area is generally tiled only once, or twice

in the overlap between plates. The fraction missed is higher in higher density regions, e.g., for galaxies with two other targets within 55 arcsec, the chance of obtaining an SDSS redshift is half that of galaxies with no close neighbours (figure 3 of Baldry et al. 2006). This is not true for GAMA because each area is tiled 4 or more times, close targets are given a higher priority in early visits, and high completeness is a primary goal (Robotham et al. 2010).

## 2.2 Distances

From the 114 441 galaxies in the  $r$ -band magnitude limited Main Survey we choose galaxies with reliable redshifts (redshift quality values of  $Q \geq 3$ ), in the range  $0.01 < z < 0.15$ , which results in a sample of 34 102 galaxies, from which we search for isolated galaxies and satellites. In the low redshift regime of this galaxy sample, the recessional velocities of galaxies are significantly affected by peculiar motions which can cause distance estimates to be in error, if simply assuming Hubble flow velocities (Masters et al. 2004). To mitigate the effects of peculiar motions on distance we make use of a parametric model of the local velocity field known as the multi-attractor model of Tonry et al. (2000).

## 2.3 Photometry

The photometry used in this paper includes *gri* Petrosian magnitudes taken from SDSS DR6 and Kron-like AUTO magnitudes measured using SExtractor (Bertin & Arnouts 1996), from our own re-reduction of the SDSS images described in Hill et al. (2011). In brief the photometry for the SDSS is obtained for five broad-band filters (*ugriz*) using a dedicated 2.5-m telescope at Apache Point, New Mexico, equipped with a mosaic CCD camera (Gunn et al. 1998) and calibrated with a 0.5-m telescope (Hogg et al. 2001). For greater detail regarding the SDSS the reader is referred to York et al. (2000) and Stoughton et al. (2002).

Unless otherwise stated, absolute magnitudes are calculated from GAMA AUTO mags such that:

$$M = m_{\text{AUTO}} - 5 \log_{10} D_L - 25 - A - K \quad (1)$$

where  $m_{\text{AUTO}}$  is the apparent AUTO magnitude of a galaxy,  $D_L$  is the luminosity distance in Mpc,  $A$  is the Galactic extinction from Schlegel et al. (1998) and  $K$  the K-correction to  $z = 0.0$ , determined using the K-Correct v4.1.4 code of Blanton & Roweis (2007). For the  $\sim 700$  galaxies where SExtractor has failed to assign an AUTO mag in any of the  $g, r, i$ -bands we use the Petrosian magnitude ( $m_{\text{Petro}}$ ) to calculate absolute magnitudes.

In the next sections we describe the criteria and methods used in the search for isolated and satellite galaxies.

## 3 SELECTION OF SATELLITE SYSTEMS

### 3.1 Isolated Galaxies

Before searching for satellites we must define a set of criteria to search for isolated galaxies which may host them. In previous papers isolated galaxies are usually found by searching for galaxies which have no neighbours brighter

than a given magnitude (either apparent or absolute) contained within a cylinder, determined by a velocity and projected radius (Zaritsky et al. 1993; Sales & Lambas 2004; Bailin et al. 2008; Ann et al. 2008). Instead of using an isolation criteria that depends solely on luminosity, here we use a criterion that also takes into account an estimate of the galaxies' stellar masses, which makes the selection more physically motivated.

To determine stellar masses we use an expression based on the relationship between a galaxy's  $(g - i)$  colour and  $i$  band stellar mass-to-light ratio ( $\mathcal{M}_*/L$ ) from Taylor et al. (2011), which is given by:

$$\log_{10} \mathcal{M}_* = -0.68 + 0.73(g - i) - 0.4(M_i - 4.58) \quad (2)$$

Here  $\mathcal{M}_*$  is the stellar mass of the galaxy in solar units ( $\mathcal{M}_*/\mathcal{M}_{\text{solar}}$ ),  $(g - i)$  is the rest-frame colour, and  $M_i$  the absolute  $i$ -band magnitude of the galaxy calculated using GAMA AUTO magnitudes. This way of estimating stellar masses has the advantage of only using two luminosities in a transparent way, unlike estimating stellar masses determined via SED fitting; and several authors have recently suggested that  $\mathcal{M}_*/L$  correlates most reliably with  $g - i$  (Gallazzi & Bell 2009; Zibetti et al. 2009; Taylor et al. 2010).

The central 95 per cent of the rest-frame  $(g - i)$  colour distribution of the galaxy sample considered in this study corresponds to  $0.26 < (g - i) < 1.24$ , implying that the galaxy stellar mass-to-light ratio in the  $i$ -band typically varies by as much as a factor of 5 from 0.32 to 1.68. In order to be robust against colour errors we restrict the mass-to-light ratio to this range.

In the search for isolated centrals we limit ourselves to using galaxies with  $r_{\text{Petro}} \leq 19.4$  in GAMA fields G09 and G15, and  $r_{\text{Petro}} \leq 19.8$  in GAMA field G12. In order to be considered isolated, the centrals must not have any comparably massive neighbours within a large surrounding region. We define isolated galaxies as those which have:

- (i) A stellar mass more than 3 times that of any neighbours ( $\mathcal{M}_{*,\text{Iso}} > 3\mathcal{M}_{*,\text{Neighbour}}$ ), within a projected radius of  $R_p \leq 1$  Mpc and  $|c\Delta z| \leq 500 \text{ km s}^{-1}$ .

- (ii) An apparent  $r$ -band Petrosian magnitude such that:

$$r_{\text{Petro}} < r_{\text{lim}} - 2.5(\log_{10} 3) - \Delta r \quad (3)$$

with  $r_{\text{lim}}$  being 19.4 for G09 and G12 or 19.8 for G15 and where  $\Delta r$  is given by:

$$\Delta r = 2.5[\log_{10}(\mathcal{M}_*/L_r)_{\text{max}} - \log_{10}(\mathcal{M}_*/L_r)] \quad (4)$$

and  $(\mathcal{M}_*/L_r)_{\text{max}}$  is a 'maximum' mass-to-light ratio in the  $r$ -band.  $r$ -band mass to light ratios are determined by dividing the stellar masses by absolute  $r$ -band Petrosian luminosities in solar units. This maximum stellar mass ratio is chosen to have the value  $(\mathcal{M}_*/L_r)_{\text{max}} = 2.14$ . The purpose of this condition is that it ensures that isolated galaxies are sufficiently brighter than the limit of the field, such that even neighbouring galaxies with the highest mass-to-light ratios that are fainter than the limit still have a stellar mass that is a factor 3 less than that of the central.

- (iii) A projected distance greater than 0.5 Mpc from each edge of the survey regions. This third condition ensures  $> 80\%$  of the area of the 1 Mpc circle surrounding a galaxy is within the survey region.

We find that 7288 galaxies out of the 34102 galaxies satisfy the second and third conditions, and overall we find 3536 galaxies to be isolated. As this study is focused on satellites hosted by typical galaxies and not those in large groups and clusters, we remove all 22 galaxies with  $\log_{10} \mathcal{M}_* \geq 11.5$  that may be brightest cluster galaxies, resulting in a sample of 3514 isolated galaxies.

### 3.2 Satellite Galaxies

After finding isolated systems we search for satellites around these galaxies. We define satellite galaxies as those surrounding isolated galaxies, which have a stellar mass that is at most one-third that of the central galaxy ( $\mathcal{M}_* < 1/3\mathcal{M}_{*,cen}$ ), within a projected radius of  $R_{Proj} \leq 500$  kpc and  $|c\Delta z| \leq 500 \text{ km s}^{-1}$ . We chose a minimum host to satellite mass ratio of 3:1 as Hopkins et al. (2008b) find that a 3:1 mass ratio merger event is the limit for an  $L^*$  disk to survive as a disk galaxy. A satellite with one-third the mass of its host will be  $\sim 1.2$  mags fainter, assuming it has the same stellar mass-to-light ratio.

Out of the 3514 isolated galaxies we find that 1426 host a total of 2998 satellite galaxies. Noting that the more massive isolated galaxies are more likely to have satellites, and the more massive hosts are more likely to have multiple satellites, simply because of the selection, we find that most (59.4 per cent) have no satellites and the mean number of satellites per isolated galaxy is 0.85. Excluding the isolated galaxies which do not host satellites we find that the mean number of satellites per central host is 2.10. Varying the projected radii and velocity differences in the isolation and satellite search criteria results in slightly different numbers of satellites per host and per isolated galaxy.

### 3.3 Other Small Neighbours

For the purposes of determining how the properties of satellite galaxies depend on the host properties, we produce a comparative sample of smaller neighbouring galaxies with similar masses to the satellites, which satisfy the same criteria but with projected distances in the range  $0.5 \leq R_{Proj} \leq 1$  Mpc. To ensure these neighbouring galaxies have no host, we check to see that these neighbouring galaxies have no nearby galaxies which are greater than 3 times the stellar mass of the small neighbour, within  $R_p < 500$  kpc and with  $|c\Delta z| < 500 \text{ km s}^{-1}$ . As these galaxies are selected in a similar way to the satellites, we consider this to be a control sample. Surrounding the 3514 isolated galaxies we find a total of 2304 of these small neighbours.

## 4 RED AND BLUE POPULATIONS OF GALAXIES

In this paper we make use of the well known colour bimodality of galaxies (Strateva et al. 2001; Baldry et al. 2004) to divide the hosts and satellite galaxies into red and blue populations, with a colour-mass diagram (CMD). This enables us to compare the properties between the populations, to examine how the radial distribution of satellites depends on

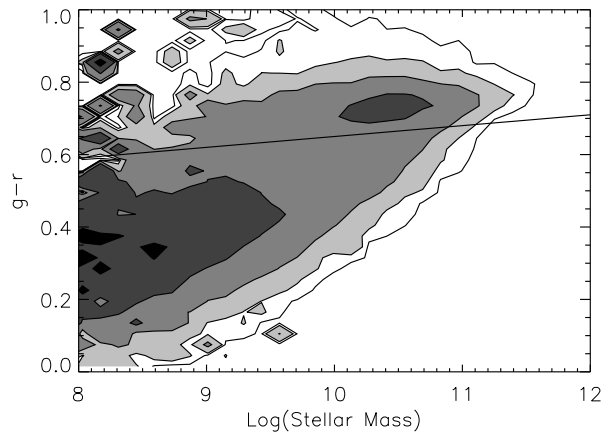


**Figure 1.**  $g-r$  colour-mass diagram for the entire sample of 34102 galaxies within  $0.01 < z < 0.15$  from the  $r$ -band limited Main Survey. The data points are weighted by  $1/V_{max}$  and represented as a logarithmic contour plot. Red and blue populations are separated by the line  $(g-r) = 0.03(\log_{10} \mathcal{M}_*) + 0.35$ .

host colour, and to determine how the red fraction of satellite galaxies varies as a function of both projected radial distance from the host and stellar mass.

### 4.1 Colour-Mass Distributions

Using  $g-r$  calculated from the AUTO mags, we produce a CMD using the sample of 34102 galaxies in the range  $0.01 < z < 0.15$ . Figure 1 shows the CMD plotted as logarithmically spaced contours. Each data point is weighted by  $1/V_{max}$ , where  $V_{max}$  is the maximum comoving volume, within which the galaxy could lie depending on its redshift and the limits of the survey (Schmidt 1968).

Colour bimodality can clearly be seen in Figure 1, and we choose to separate the red and blue populations using a straight line with the equation:

$$(g-r) = 0.03(\log_{10} \mathcal{M}_*) + 0.35. \quad (5)$$

Figure 1 looks almost identical to the CMD in figure A1 of van den Bosch et al. (2008), produced using stellar masses derived from Bell et al. (2003). CMDs for the isolated galaxies, central hosts and satellites with projected distances of  $R_{Proj} \leq 500$  kpc can be seen in Figure 2, which clearly shows that the majority of isolated galaxies which host satellites are red (906 out of 1426 hosts). Out of the 2998 satellites we find 1097 red and 1901 blue galaxies. By further dividing the sample into red/blue satellite/host systems, we find that 41.2 per cent (1235) of the satellites are blue with red hosts, 33.3 per cent (998) are red satellites with red hosts, 22.2 per cent (666) are blue satellites with blue hosts, and only 3.3 per cent (99) are red satellites with blue hosts. Overall the blue fraction of satellites is 63.4 per cent, which rises to 87.1 per cent for blue hosts compared to 55.3 per cent for red hosts.

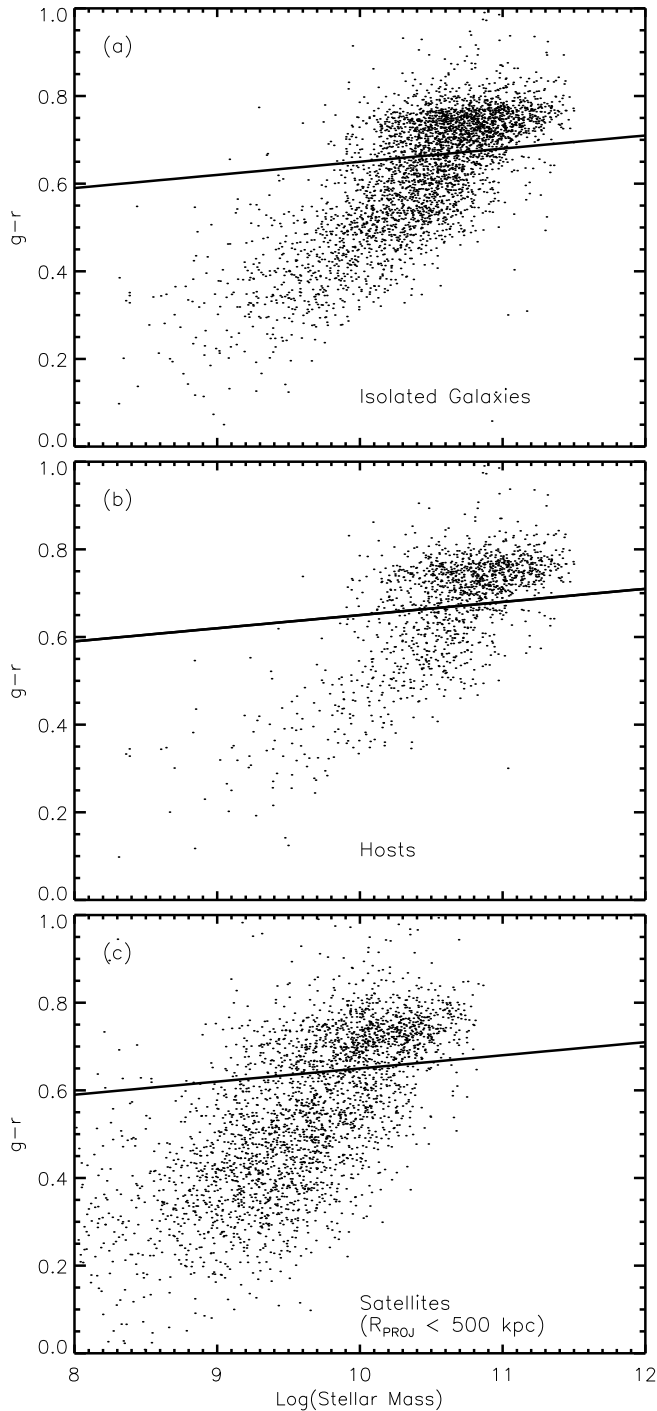


**Figure 2.**  $g-r$  colour-mass diagrams for (a) the 3514 isolated galaxies (b) the 1426 central hosts and (c) 2998 satellites. Red and blue populations are separated by the line  $(g-r) = 0.03(\log_{10} \mathcal{M}_*) + 0.35$ .

## 4.2 Luminosity and Mass Distributions

In this section we compare the properties of the different samples of galaxies. In Figure 3 we show the distributions in luminosity and stellar mass for red and blue hosts and satellites. This shows, as expected, the red population on average being more luminous and massive than the blue population. We calculate mean stellar masses and absolute  $r$ -band magnitudes for red host galaxies as  $\log_{10} \mathcal{M}_* = 10.81$  and  $M_r = -21.81$  respectively, compared to  $\log_{10} \mathcal{M}_* = 10.31$  and  $M_r = -21.28$  for the blue hosts. The latter is similar to the value for the Milky Way, and the Schechter break ( $M^*$ ) of blue galaxies (Loveday et al. 2011 in preparation). Similarly for the red satellites we calculate means of  $\log_{10} \mathcal{M}_* = 10.00$  and  $M_r = -19.96$ , and  $\log_{10} \mathcal{M}_* = 9.35$  and  $M_r = -19.30$  for the blue. Both populations are typically more massive and luminous than the Large Magellanic Cloud.

Comparing the host galaxies to isolated galaxies without satellites, we find that both the blue and red galaxies with satellites are more massive and more luminous than those without, which is most likely a result of our satellite selection as the more massive isolated galaxies have a larger chance of hosting a satellite. The average mass and luminosity of the red galaxies without satellites is  $\log_{10} \mathcal{M}_* = 10.61$  and  $M_r = -21.39$  compared to the blue galaxies which have  $\log_{10} \mathcal{M}_* = 10.12$  and  $M_r = -20.94$ .

The mean masses and luminosities of the small neighbours are very similar to those of the satellites and we find means of  $\log_{10} \mathcal{M}_* = 10.77$  and  $M_r = -20.17$  for red galaxies and  $\log_{10} \mathcal{M}_* = 9.42$  and  $M_r = -19.48$  for the blue. This is reassuring as it means that the small neighbours do indeed have similar properties to the satellites and can be considered a ‘control’ sample, allowing comparisons between the two.

Other quantities useful for comparison with cosmological models include the stellar mass and luminosity differences between hosts and satellites. In Figure 4 we show histograms of these quantities for the blue and red hosts.

Due to our satellites having stellar masses that are less than 1/3 of their host mass,  $\Delta \log_{10} \mathcal{M}_*$  has a minimum value of 0.477, and we find a maximum of  $\Delta \log_{10} \mathcal{M}_* = 3$  (1/1000th the mass of the host). We find that the average satellite in this study is  $\sim 1/10$ th of the mass of the host and calculate mean logarithmic mass differences of 1.05 and 1.39 for red and blue satellites with red hosts, and 0.95 and 1.11 for red and blue satellites with blue hosts.

As for luminosity difference, we find that satellites are typically  $\sim 2$  magnitudes fainter than their hosts. Red and blue satellites of red hosts, are both found to have mean magnitude differences of 2.37, and red and blue satellites with blue hosts have magnitude differences of 2.54 and 2.21. We also find a small fraction of satellites which have a negative value of  $\Delta M_r$  and are brighter than their hosts, which would be missed by other studies. In other words, when considering red hosts, they can be more than three times more massive than their blue satellites yet be of similar luminosity.

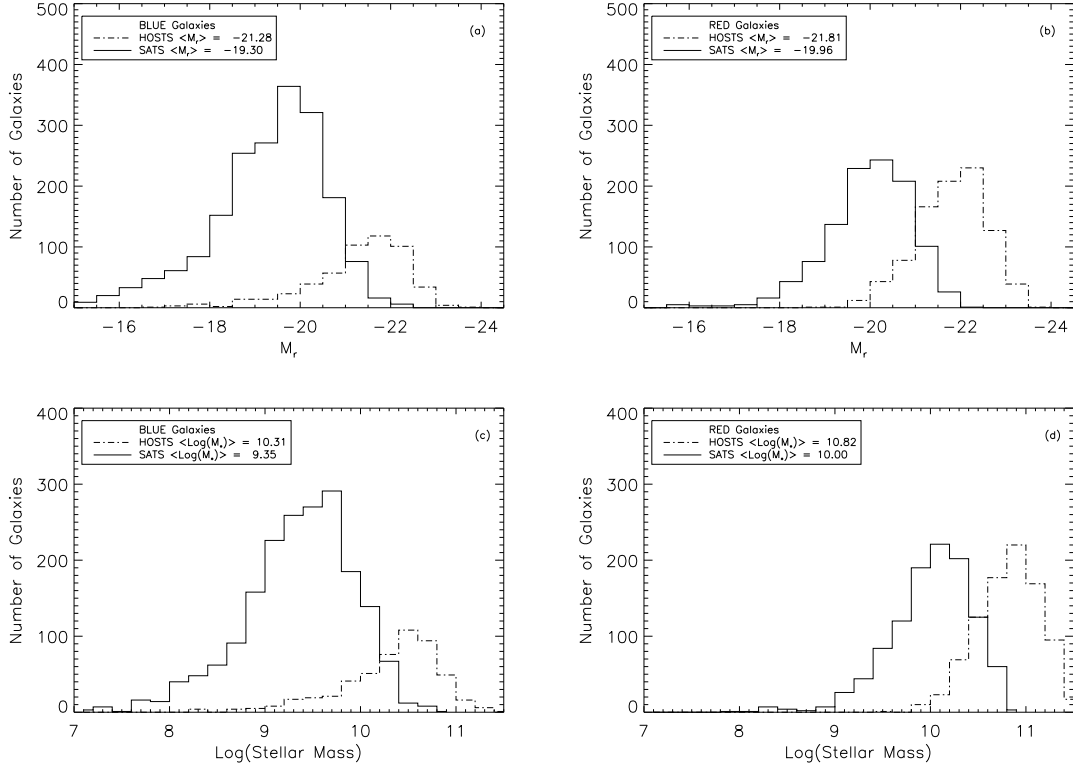


**Figure 3.** Histograms showing the distribution of  $r$ -band absolute magnitudes (a,b) and stellar masses (c,d) for the blue and red populations of satellites with  $R_{Proj} \leq 500$  kpc (solid lines) and host galaxies (dashed lines).

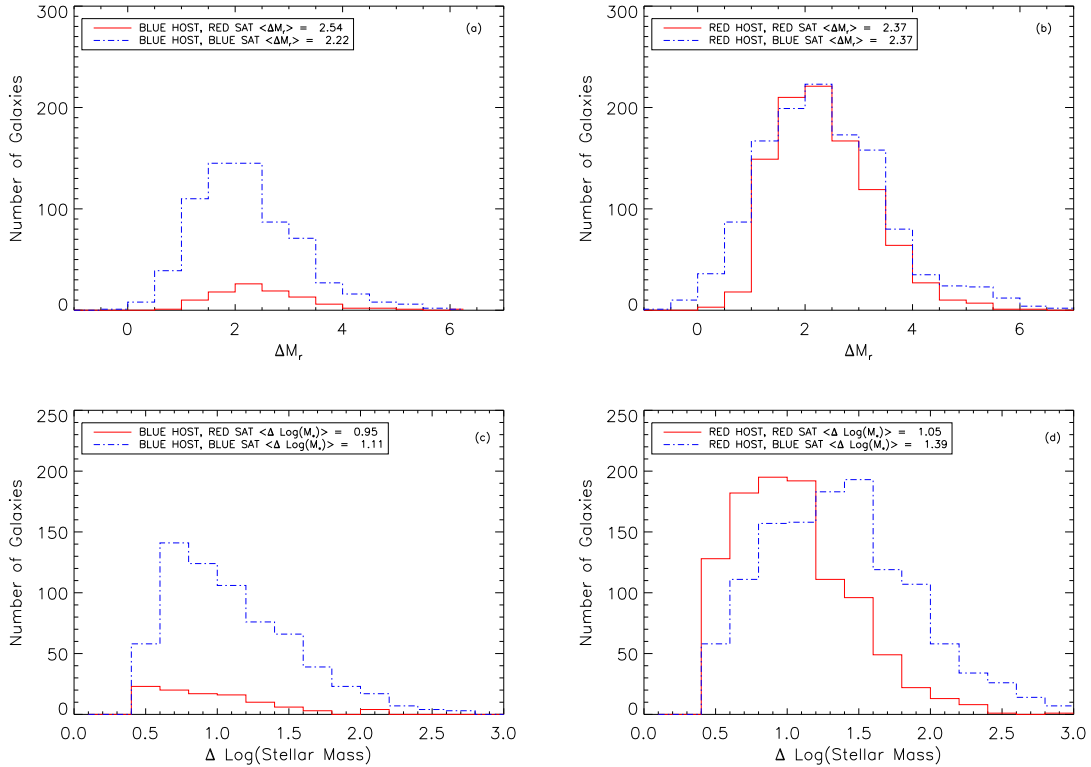


**Figure 4.** Distributions of the differences in the absolute  $r$ -band magnitude (a,b) and stellar masses (c,d) between the red and blue satellites ( $R_{Proj} \leq 500$  kpc) and their red and blue central hosts. Histograms for red satellites are shown as dotted lines, blue satellites are shown as dotted-dashed lines.

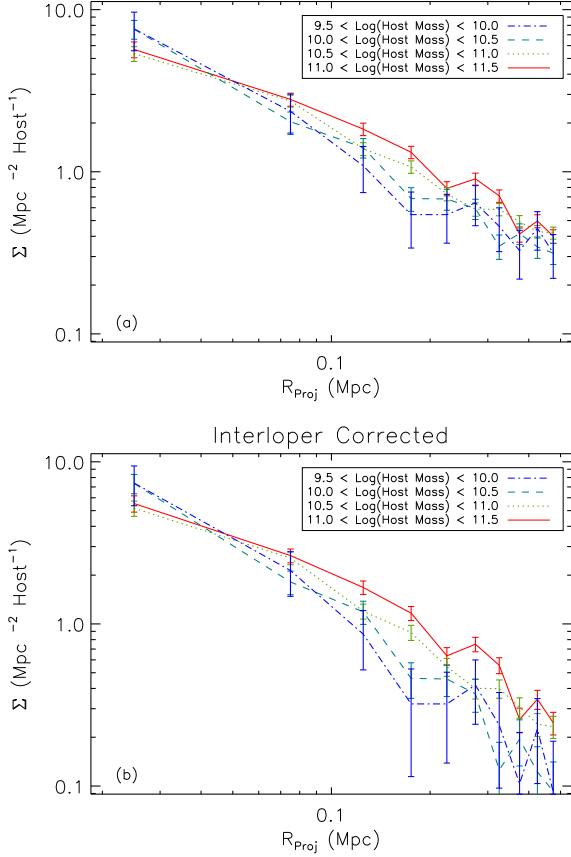


**Figure 5.** (a): Projected densities of satellites with  $R_{Proj} \leq 500$  kpc, divided into four host stellar mass bins, using projected radius bins of width  $\Delta R = 0.05$  Mpc. (b): The same as above corrected for interlopers. The error bars shown are Poissonian.

## 5 PROJECTED DENSITY OF SATELLITES

To investigate the radial distribution of the satellites we calculate the projected density per host given by:

$$\Sigma(R) = \frac{N_{Sat}(R)}{\pi N_{Host}(R_2^2 - R_1^2)} \quad (6)$$

where  $N_{Sat}(R)$  is the number of satellites found within a shell bounded by inner and outer projected radii,  $R_1$  and  $R_2$ , from the host and  $N_{Host}$  is the number of host galaxies and  $R$  is the midpoint of the bin.

Using projected radius bins of width  $\Delta R = 0.05$  Mpc and dividing the satellites into four host stellar mass bins;  $9.5 < \log_{10} \mathcal{M}_* < 10.0$ ,  $10.0 < \log_{10} \mathcal{M}_* < 10.5$ ,  $10.5 < \log_{10} \mathcal{M}_* < 11.0$  and  $11.0 < \log_{10} \mathcal{M}_* < 11.5$ , we produce Figure 5(a) which shows how the projected density of galaxies varies as a function of projected distance. We fit the projected density with a power law, parametrized by a slope,  $\alpha$ , and normalisation  $A$ :

$$\Sigma(R) = A(R/\text{Mpc})^\alpha. \quad (7)$$

with  $A$  in  $\text{Mpc}^{-2}$  as  $\Sigma$  is in  $\text{Mpc}^{-2}$ .

In Table 1 we show the best-fitting parameters and errors for each of the curves, and find that there is little variation in the best-fitting slope, which steepens slightly from  $\alpha = -0.94 \pm 0.04$  for satellites with hosts in the

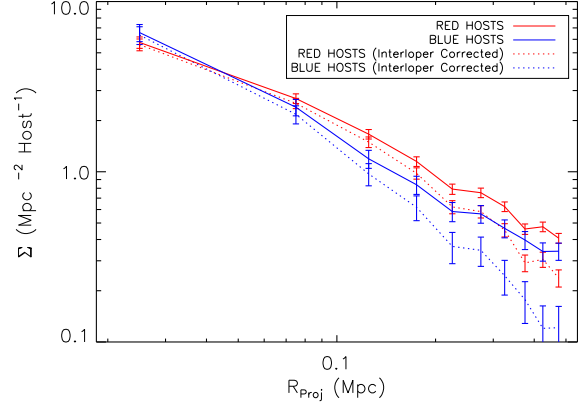


**Figure 6.** Projected densities of satellites with  $R_{Proj} \leq 500$  kpc, for the red and blue hosts with masses in the range  $9.5 \leq \log_{10} \mathcal{M}_* \leq 11.5$ , using projected radius bins of width  $\Delta R = 0.05$  Mpc. The interloper corrected values are connected by dotted lines. The error bars are Poissonian.

mass range  $11.0 < \log_{10} \mathcal{M}_* < 11.5$ , through to  $\alpha = -1.06 \pm 0.03$  for satellites with hosts in the mass range  $9.5 < \log_{10} \mathcal{M}_* < 10.0$ . Dividing the satellites into those with red and blue hosts (Figure 6), with host masses between  $9.5 < \log_{10} \mathcal{M}_* < 11.5$ , we find a best fitting slope of  $\alpha = -0.94 \pm 0.03$  for satellites with red hosts compared to those with blue host which have  $\alpha = -1.04 \pm 0.04$ . These slopes suggest that the blue, low mass host galaxies have slightly more centrally concentrated satellites. The slopes however are affected by interlopers, galaxies which are mistaken as satellites by projection and not actually bound to their hosts.

In order to correct for interlopers we use a simple method of subtracting the average projected density of the small neighbours, with projected radii in the range  $0.5 < R_{Proj} < 1.0$  Mpc, from the projected density of the satellites in each bin:

$$\Sigma(R)_{\text{Int Corr}} = \Sigma(R)_{\text{Sat}} - \langle \Sigma(0.5 < R < 1.0)_{\text{small neigh}} \rangle. \quad (8)$$

Note that this assumes that these galaxies in the 0.5–1 Mpc annuli represent the average large-scale or ‘super cluster’ environment around the hosts, and the correction will be an overestimate in hosts where a significant bound satellite population extends beyond 0.5 Mpc, in particular for our most massive host sample (11.0–11.5).

The result of applying this interloper correction and fitting the slope for each of the host mass ranges (and colour) can also be seen in Table 1, which shows that the best-fitting slope now significantly varies with host mass and steepens from  $\alpha = -1.09 \pm 0.04$  for satellites with hosts in the mass range  $11.0 < \log_{10} \mathcal{M}_* < 11.5$  through to  $\alpha = -1.4 \pm 0.1$  for satellites with hosts in the mass range  $9.5 < \log_{10} \mathcal{M}_* < 10.0$ . For the red and blue hosts, we obtain interloper corrected slopes of  $\alpha = -1.13 \pm 0.03$  and  $\alpha = -1.38 \pm 0.04$  respectively. The results of this interloper subtraction can be seen in Figure 5(b) and as the dotted lines in Figure 6.

An observed decline in the projected density, which overall can be approximated by  $\Sigma(R) \propto R^{-1}$ , is similar to other studies that investigate the radial distribution of satellites. For example, Lorrimer et al. (1994) using



**Table 1.** Best fitting  $A$  and  $\alpha$  parameters (Equation 7) for the projected densities in Figure 5 and Figure 6, corrected and uncorrected for interlopers. The uncertainties quoted are derived from least-squares straight-line fits to  $\log \Sigma$  versus  $\log R$  with the data points shown in the figures.

Host Stellar Mass Range	$N_{\text{Sat tot}}$	$A_{\text{un corr}} \text{ (Mpc}^{-2}\text{)}$	$\alpha_{\text{un corr}}$	$A_{\text{Int corr}} \text{ (Mpc}^{-2}\text{)}$	$\alpha_{\text{Int corr}}$
$9.5 \leq \log_{10} \mathcal{M}_* \leq 10.0$	111	$0.14 \pm 0.03$	$-1.06 \pm 0.10$	$0.05 \pm 0.01$	$-1.40 \pm 0.10$
$10.0 \leq \log_{10} \mathcal{M}_* \leq 10.5$	457	$0.13 \pm 0.01$	$-1.09 \pm 0.05$	$0.04 \pm 0.04$	$-1.46 \pm 0.05$
$10.5 \leq \log_{10} \mathcal{M}_* \leq 11.0$	1 225	$0.20 \pm 0.01$	$-0.94 \pm 0.03$	$0.10 \pm 0.01$	$-1.14 \pm 0.04$
$11.0 \leq \log_{10} \mathcal{M}_* \leq 11.5$	1 140	$0.23 \pm 0.02$	$-0.94 \pm 0.04$	$0.14 \pm 0.01$	$-1.09 \pm 0.04$
ALL BLUE HOSTS	700	$0.14 \pm 0.01$	$-1.04 \pm 0.04$	$0.05 \pm 0.01$	$-1.38 \pm 0.04$
ALL RED HOSTS	2 223	$0.21 \pm 0.01$	$-0.94 \pm 0.03$	$0.12 \pm 0.01$	$-1.13 \pm 0.03$

the Centre for Astrophysics redshift survey, find a slope of  $\alpha = -0.91 \pm 0.05$  for satellites with magnitudes in the range  $-16 < B < -18$ , after correcting for background galaxies, which is slightly shallower than the interloper corrected slopes we obtain. Furthermore, they divide their satellite sample into early- and late-type hosts, to find that satellites with early-type hosts are more centrally concentrated than late types, finding slopes of  $\alpha = -1.01 \pm 0.1$  for satellites of early-type hosts and  $\alpha = -0.78 \pm 0.05$  and for the late-type hosts, which is the opposite to what we find. Although our slope for satellites of red hosts is consistent with their result for early-type hosts, our result for the satellites of blue galaxies differs from their findings for late-type hosts.

More recently, Chen et al. (2006) find an interloper corrected slope of  $\alpha = -1.58 \pm 0.11$ , using a galaxy sample from SDSS DR4. Here satellites are defined as galaxies with  $M_r < -18.0$ , which are 2 mags fainter than their hosts, with  $R_{\text{Proj}} \leq 500$  kpc and  $\Delta V \leq 500 \text{ km s}^{-1}$  and isolated galaxies are defined as those with  $M_r \leq -20.0$ , have no nearby galaxies within  $\Delta m \leq 2$  mag,  $\Delta V \leq 1000 \text{ km s}^{-1}$  and  $R_{\text{Proj}} \leq 500$  kpc. Using these same selection criteria and a larger data sample from SDSS DR6, Chen (2008) find that the interloper corrected slopes of satellites of red and blue hosts are almost identical and obtain values of  $\alpha = -1.54 \pm 0.12$  and  $\alpha = -1.50 \pm 0.12$  for satellites of blue hosts and red hosts, respectively. Although these values are similar to our slopes for the blue and low-mass hosts, they are quite different for the red and high-mass hosts. Chen (2008) and others have used  $r$ -band luminosity for isolation criteria. For red hosts, this is significantly more stringent than using an estimated stellar mass that allows for equally luminous blue satellites. This could explain some of these differences.

Sales et al. (2007) using a sample of galaxies from the semi-analytic Millennium Simulation find a slope of  $\alpha = -1.55 \pm 0.08$ , for satellites again that are at least 2 magnitudes fainter than their hosts, within  $R_{\text{Proj}} \leq 500$  kpc and  $\Delta V \pm 500 \text{ km s}^{-1}$ .

Investigating the satellites of 34 elliptical galaxies Madore et al. (2004) find a decline with a slope of  $\alpha = -0.5$  out to  $R_{\text{Proj}} \simeq 150$  kpc, which flattens out at greater projected radii. Although the slope they obtain is again inconsistent with our results, this may be due to the small numbers of galaxies involved. They do note that there is a flattening in the projected density at  $R_{\text{Proj}} \geq 300$  kpc, which can also be seen in our data.

Finally, Ann et al. (2008) using SDSS DR5 data, define satellites as galaxies with  $M_r < -18.0$ , which are more than 1 mag fainter in the  $r$ -band than their hosts, within  $R_{\text{Proj}} \leq 1$  Mpc and  $\Delta V \leq 1000 \text{ km s}^{-1}$ . They also use an isolation criterion, so that isolated galaxies are required to have  $M_r < -19.0$ , and no neighbours within  $\Delta m \leq 1$  mag of the host, within a  $R_{\text{Proj}} \leq 500$  kpc and  $\Delta V \pm 500 \text{ km s}^{-1}$ , producing a sample of 2 254 hosts with 4 986 satellites. Without correcting for interlopers they fit slopes for satellites within  $R_{\text{Proj}} = 200$  kpc of their hosts, and obtain values of  $\alpha \sim -1.8$  for both the late- and early-type satellites of late-type hosts and for the early-type satellites of early-type hosts. For the late-type satellites of early-type hosts a shallower slope of  $\alpha \sim -1.5$  is found.

The shallower slopes for the high-mass hosts compared to low-mass hosts measured over the range 0.05–0.5 Mpc are expected if satellite density profiles are related to dark-matter profiles (Navarro, Frenk & White 1996, hereafter NFW; surface density profile given by Bartelmann 1996). The higher-mass hosts would be expected to have larger NFW scale radii and therefore shallower dark-matter profiles over the radial range probed by our study.

## 6 RED FRACTION OF SATELLITE GALAXIES

After measuring the projected density of satellites, we determine how the red fraction of satellites varies as a function of mass and projected distance from the hosts. It should be noted that the most robust results, free of significant selection effects, are the differences between the satellites and small neighbours.

### 6.1 Red Fraction as a Function of Projected Distance

To measure the red fraction of satellites ( $R_{\text{Proj}} \leq 0.5$  Mpc) and small neighbours ( $0.5 \leq R_{\text{Proj}} \leq 1$  Mpc) we divide the number counts of red galaxies by the total number of galaxies in bins of projected radius of width  $\Delta R_{\text{Proj}} = 0.1$  Mpc. By dividing the sample of satellites into those with red and blue hosts we produce Figure 7(a). By dividing the sample of satellites into four bins of host stellar mass as before, we produce Figure 7(b). The error bars on the red fraction of galaxies in all plots are  $1\sigma$  beta distribution confidence intervals explained in detail in Cameron (2010). These are an improvement over other methods for estimating binomial

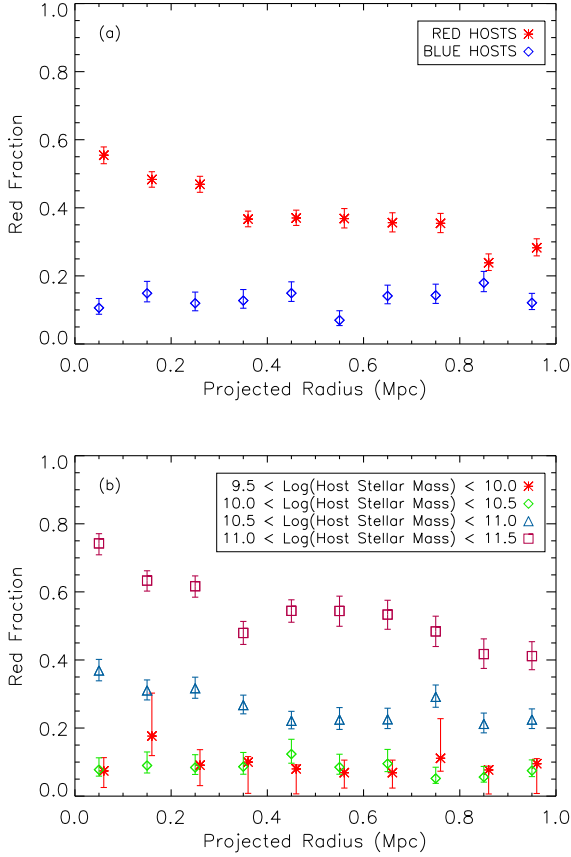


**Figure 7. (a):** The red fraction of satellite galaxies as a function of projected radius for the red and blue hosts. **(b):** The red fraction of satellite galaxies as a function of projected radius, for four different host stellar mass ranges. We define galaxies with  $R_{Proj} \leq 0.5$  Mpc as satellites and galaxies with  $0.5 \leq R_{Proj} \leq 1.0$  Mpc as small neighbouring galaxies which have been selected in a similar way. The error bars shown are  $1\sigma$  beta distribution confidence intervals.

confidence intervals, such as Poisson errors, which are liable to misrepresent the degree of statistical uncertainty for small samples, or fractions that approach values of 0 or 1.

From Figure 7(a) it is clear that the red fraction of satellites of red hosts is significantly higher than those with blue hosts. The average red fraction of all the points between  $0.05 \leq R_{Proj} \leq 1$  Mpc for the satellites of red hosts is 0.38 compared to 0.13 for the blue hosts. The red fraction of satellites for red hosts increases by a factor of 1.49 from 0.37 at  $R_{Proj} = 0.45$  Mpc to 0.55 at 0.05 Mpc. For the satellites of blue hosts no trend in the red fraction as a function of radius is seen.

Similar trends are reflected in Figure 7(b) as expected. The red fraction of satellites and small neighbours increases significantly as a function of host mass, from an average red fraction of all the points between  $0.05 \leq R_{Proj} \leq 1$  Mpc of 0.09 for galaxies associated with hosts with  $9.5 \leq \log_{10} \mathcal{M}_* \leq 10.0$ , 0.08 for galaxies of hosts with  $10.0 \leq \log_{10} \mathcal{M}_* \leq 10.5$ , 0.27 for galaxies of hosts with  $10.5 \leq \log_{10} \mathcal{M}_* \leq 11.0$ , through to 0.54 for galaxies of hosts with  $11.0 \leq \log_{10} \mathcal{M}_* \leq 11.5$ . The highest two host

mass ranges show that an upturn in the red fraction occurs within  $R_{Proj} \sim 500$  kpc. For the highest host mass bin  $11.0 \leq \log_{10} \mathcal{M}_* \leq 11.5$ , the red fraction of satellites increases by a factor of 1.4 from 0.54 at  $R_{Proj} = 0.45$  Mpc to 0.74 at 0.05 Mpc and for satellites with host masses of  $10.5 \leq \log_{10} \mathcal{M}_* \leq 11.0$ , with the red fraction increasing by a factor of 1.7 from 0.22 at  $R_{Proj} = 0.45$  Mpc to 0.37 at 0.05 Mpc. No trend in the red fraction as a function of radius is observed for the 2 lowest host mass bins.

Following on from this we investigate how the red fraction varies as a function of satellite mass, by subdividing galaxies in the host mass bins above further into satellite mass bins. It is important to do this in order to verify that the satellite trends are not simply due to mass segregation, and to separate ‘environment quenching’ from ‘mass quenching’ (Peng et al. 2010). Figure 8(a,c,e) shows how the red fraction varies as a function of radius, with the data separated into 3 different plots for three different host mass bins, and then subdivided into satellite mass bins of  $9.5 \leq \log_{10} \mathcal{M}_* \leq 10.0$ ,  $10.0 \leq \log_{10} \mathcal{M}_* \leq 10.5$ ,  $10.5 \leq \log_{10} \mathcal{M}_* \leq 11.0$  and  $11.0 \leq \log_{10} \mathcal{M}_* \leq 11.5$ , depending on the host mass bin. The mean numbers of satellites and small neighbours in each bin are 36.2, 65.6 and 48.5 for those with host masses in the ranges  $10.0 \leq \log_{10} \mathcal{M}_* \leq 10.5$ ,  $10.5 \leq \log_{10} \mathcal{M}_* \leq 11.0$  and  $11.0 \leq \log_{10} \mathcal{M}_* \leq 11.5$  respectively. In Table 2 we show the average red fractions of satellites and small neighbours for each of the different host and satellite mass ranges. From these it can be seen that:

- For satellites with hosts in the range  $10.0 \leq \log_{10} \mathcal{M}_* \leq 10.5$ , little change in the red fraction as a function of radius is observed, with the red fraction of the satellites and small neighbours remaining around the 0.05 level for galaxies with  $9.0 \leq \log_{10} \mathcal{M}_* \leq 9.5$  and  $\sim 0.14$  for satellites with stellar masses in the range  $9.5 \leq \log_{10} \mathcal{M}_* \leq 10.0$ .
- For satellites with hosts in the range  $10.5 \leq \log_{10} \mathcal{M}_* \leq 11.0$ , the red fraction increases with satellite mass, such that the average red fraction increases from  $0.11 \pm 0.03$  for satellites with masses  $9.0 \leq \log_{10} \mathcal{M}_* \leq 9.5$ , to  $0.33 \pm 0.03$  for satellites with masses of  $9.5 \leq \log_{10} \mathcal{M}_* \leq 10.0$ , and  $0.57 \pm 0.02$  for satellites with masses of  $10.0 \leq \log_{10} \mathcal{M}_* \leq 10.5$ . It also becomes apparent that the red fraction increases as distance decreases. The average red fraction of the satellites is greater than the average red fraction of the small neighbours in the same mass range. For galaxies with  $9.0 \leq \log_{10} \mathcal{M}_* \leq 9.5$  this difference is  $0.05 \pm 0.04$ ,  $0.15 \pm 0.04$  for galaxies with  $9.5 \leq \log_{10} \mathcal{M}_* \leq 10.0$  and  $0.06 \pm 0.04$  for galaxies with  $10.0 \leq \log_{10} \mathcal{M}_* \leq 10.5$ .
- Satellites with host masses  $11.0 \leq \log_{10} \mathcal{M}_* \leq 11.5$  show similar trends and the radial dependence becomes even more apparent, especially for the low mass satellites. The average red fraction of satellites increases from  $0.37 \pm 0.07$  for satellites with  $9.0 \leq \log_{10} \mathcal{M}_* \leq 9.5$ , through to  $0.90 \pm 0.02$  for the satellites with  $10.5 \leq \log_{10} \mathcal{M}_* \leq 11.0$ . The difference between the red fraction of satellites and the small neighbours is observed to be  $0.25 \pm 0.07$  for galaxies in the mass range  $9.0 \leq \log_{10} \mathcal{M}_* \leq 9.5$ ,  $0.18 \pm 0.07$  for galaxies with  $9.5 \leq \log_{10} \mathcal{M}_* \leq 10.0$ ,  $0.15 \pm 0.05$  for galaxies with  $10.0 \leq \log_{10} \mathcal{M}_* \leq 10.5$  and  $0.15 \pm 0.04$  for galaxies with  $10.5 \leq \log_{10} \mathcal{M}_* \leq 11.0$ .

Our results here support the ‘galactic conformity’ phenomenon, whereby red/early-type centrals have a signifi-

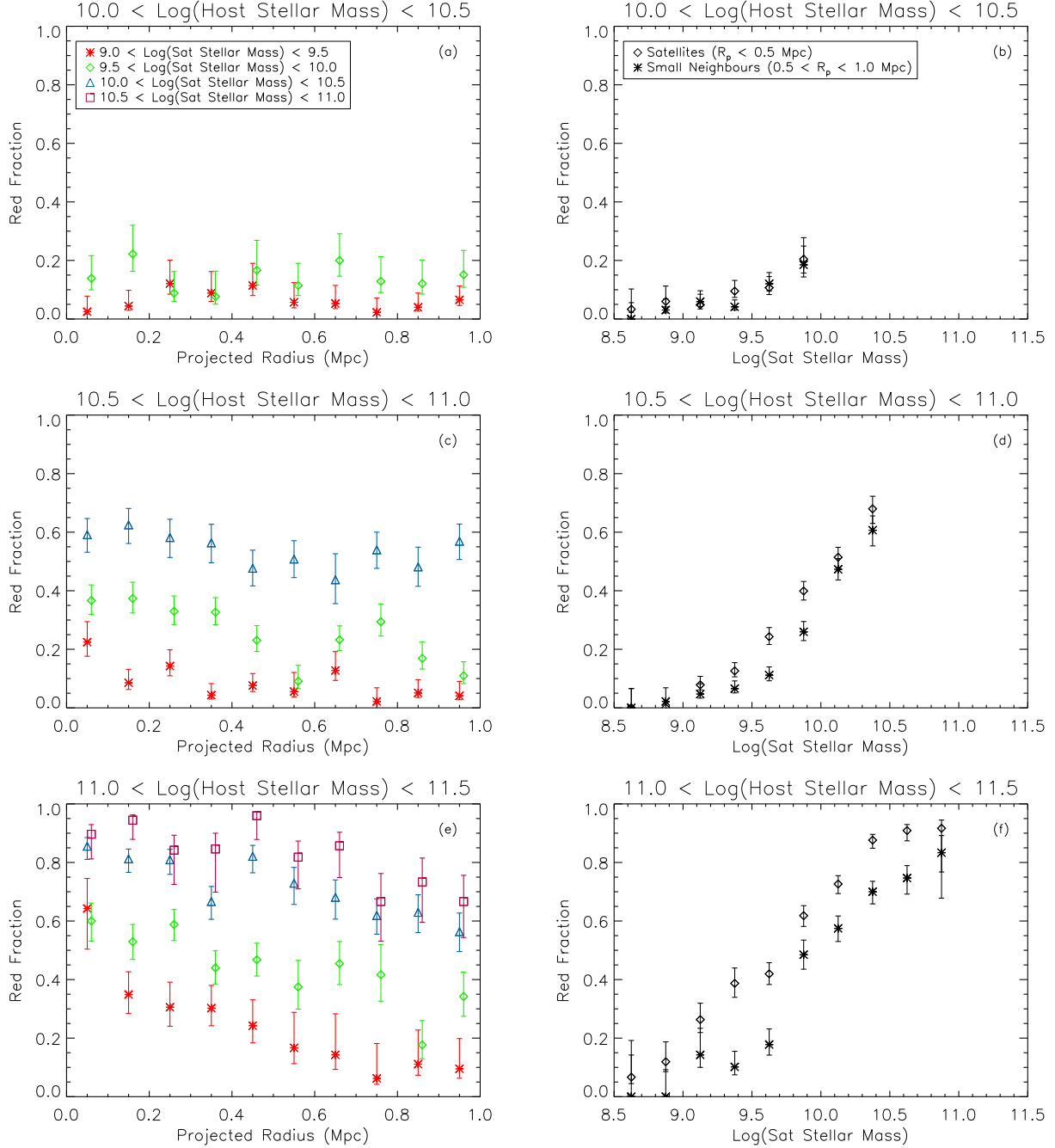


**Figure 8.** Left panels (a,c,e) show the red fraction of satellite galaxies as a function of projected radius and satellite stellar mass, shown for 3 different central host stellar mass ranges. Host masses of  $10.0 \leq \log_{10} \mathcal{M}_* \leq 10.5$ ,  $10.5 \leq \log_{10} \mathcal{M}_* \leq 11.0$  and  $11.0 \leq \log_{10} \mathcal{M}_* \leq 11.5$  with satellites of stellar masses  $9.0 \leq \log_{10} \mathcal{M}_* \leq 9.5$  (red stars),  $9.5 \leq \log_{10} \mathcal{M}_* \leq 10.0$  (green diamonds),  $10.0 \leq \log_{10} \mathcal{M}_* \leq 10.5$  (blue triangles) and  $10.5 \leq \log_{10} \mathcal{M}_* \leq 11.0$  (purple squares). Right panels (b,d,f) show the red fraction of satellites with  $R_{\text{Proj}} \leq 0.5$  Mpc and small neighbours with  $0.5 \leq R_{\text{Proj}} \leq 1.0$  Mpc as a function of satellite mass, for hosts in the same mass ranges opposite. The errors shown are  $1\sigma$  beta distribution confidence intervals.

cantly higher fraction of red/early-type satellites, noted first by Weinmann et al. (2006) and also observed by Ann et al. (2008). Weinmann et al. (2006) produce a large catalogue of  $\sim 53\,000$  groups, from a sample of  $\sim 92\,000$  galaxies from the SDSS DR2, using the halo-based group finder of Yang et al. (2005). Defining centrals as the brightest group members and satellites as the remaining group members, they deter-

mine the projected halocentric distances (normalised to the virial radius of the system  $R_{\text{vir}}$ ) of the satellites and halo masses of the systems. They find that the early-type fractions of satellites increase as a function of increasing luminosity, increasing group halo mass and decreasing halocentric distance. For halo masses with  $14 < \log_{10} \mathcal{M} < 15$ , the early-type fraction of satellites increases from  $\sim 40$  per cent

**Table 2.** Average red fraction of satellites and small neighbours of galaxies in Figure 8. The error quoted is the standard error.

Host Mass Range	Satellite Mass Range	Mean Satellite Red Fraction	Mean Small Neighbour Red Fraction
$10.0 \leq \log_{10} \mathcal{M}_* \leq 10.5$	$9.0 \leq \log_{10} \mathcal{M}_* \leq 9.5$	$0.08 \pm 0.02$	$0.04 \pm 0.01$
	$9.5 \leq \log_{10} \mathcal{M}_* \leq 10.0$	$0.14 \pm 0.03$	$0.14 \pm 0.02$
$10.5 \leq \log_{10} \mathcal{M}_* \leq 11.0$	$9.0 \leq \log_{10} \mathcal{M}_* \leq 9.5$	$0.11 \pm 0.03$	$0.06 \pm 0.02$
	$9.5 \leq \log_{10} \mathcal{M}_* \leq 10.0$	$0.33 \pm 0.03$	$0.18 \pm 0.04$
	$10.0 \leq \log_{10} \mathcal{M}_* \leq 10.5$	$0.57 \pm 0.02$	$0.51 \pm 0.02$
$11.0 \leq \log_{10} \mathcal{M}_* \leq 11.5$	$9.0 \leq \log_{10} \mathcal{M}_* \leq 9.5$	$0.37 \pm 0.07$	$0.12 \pm 0.02$
	$9.5 \leq \log_{10} \mathcal{M}_* \leq 10.0$	$0.53 \pm 0.03$	$0.35 \pm 0.05$
	$10.0 \leq \log_{10} \mathcal{M}_* \leq 10.5$	$0.79 \pm 0.03$	$0.64 \pm 0.03$
	$10.5 \leq \log_{10} \mathcal{M}_* \leq 11.0$	$0.90 \pm 0.02$	$0.75 \pm 0.04$

at  $0.9R/R_{vir}$  to  $\sim 60$  per cent at  $0.1R/R_{vir}$ . For lower-mass halos with  $12 < \log_{10} \mathcal{M} < 13$ , the early-type fraction of satellites is approximately constant at  $\sim 25$  per cent. This is a similar picture to what we see in Figure 7.

In a study more directly comparable to ours, Ann et al. (2008) investigate satellite systems of isolated hosts, who determine the morphologies of their satellite and host samples to investigate the early-type fraction of satellite galaxies as a function of radius. Splitting their hosts into early and late types, they find that the early-type satellite fraction for early-type hosts increases from  $\sim 0.2$  at  $R_{Proj} = 1$  Mpc to  $\sim 0.6$  at  $R_{Proj} = 0.05$  kpc, whereas the early-type fraction for late-type hosts remains roughly constant,  $\sim 0.2$  for all projected radii, which is almost identical to what we find in Figure 7(a). By dividing their sample into hosts with  $M_r < -20.5$  and  $-21.0 < M_r < -19.0$ , they show in their figure 2 that the brighter early-type hosts have an early-type satellite fraction which is  $0.05\text{--}0.20$  greater in each projected radius bin compared to those with fainter hosts. For the brighter host bin, the early-type satellite fraction increases from  $\sim 20$  per cent at  $R_{Proj} = 1$  Mpc to  $\sim 70$  per cent at  $R_{Proj} = 0.05$  Mpc, whereas the early-type satellite fraction for fainter hosts increases from  $\sim 20$  per cent at  $R_{Proj} = 1$  Mpc to  $\sim 60$  per cent at  $R_{Proj} = 0.05$  Mpc. For the late-type hosts, the early-type satellite fraction is roughly constant with projected radius at  $\sim 25$  per cent for hosts with  $M_r < -20.5$  compared to being roughly constant at  $\sim 15$  per cent for hosts with  $-21.0 < M_r < -19.0$ . Again this trend is similar to our result that the red fraction of satellites increases with increasing host mass.

## 6.2 Red Fraction as a Function of Mass

An alternative way of showing how the red fraction varies as a function of radius can be seen in Figure 8(b,d,f), which shows the red fraction of satellites and small neighbours in mass bins of width  $\Delta \log_{10} \mathcal{M} = 0.25$ , for the same host mass ranges as on the left-hand side. As expected the red fraction of satellites and small neighbours increases with increasing stellar mass. Figure 8(b,d,f) clearly shows that host mass has the biggest effect on the red fraction of satellites relative to the small neighbours. For the satellites with the lowest host masses ( $10.0 \leq \log_{10} \mathcal{M}_* \leq 10.5$ ), there is virtually no difference between the red fraction of the satellites and small neighbours, confirming that the red fraction has no radial dependence. For the highest mass hosts, the red fraction of

the satellites is about 0.2 greater than the red fraction of small neighbours.

Using the SDSS DR4 group catalogue of Yang et al. (2007), van den Bosch et al. (2008) define the most massive members of groups as centrals and the remaining group members as satellites, producing a sample of 218 103 centrals and 59 982 satellites. They then investigate how the red fractions of hosts (centrals) and satellites by mass compare. In their figure 8, they show that the difference in the red fraction of centrals and satellites is the greatest at low masses (the satellites have red fractions which are 20–40 per cent higher for  $\log_{10} \mathcal{M}_* \leq 10.0$ ), converging at higher masses. The significant red fraction at the lowest satellite masses is discrepant with what we observe, although this may be explained by the different definitions of satellite galaxies.

## 6.3 Discussion

We have shown that the red fraction of satellites surrounding isolated hosts increases as a function of host stellar mass, satellite mass and decreasing projected separation, indicating the quenching of star formation in satellite galaxies is more efficient in most massive systems and acts within  $\sim 500$  kpc of the host. This quenching of star formation is likely to be due to the removal of gas by a combination of radiative and gravitational effects of the host, which have been investigated in previous studies.

One way of shutting off the star formation in satellite galaxies is by strangulation (Larson et al. 1980; Balogh et al. 2000), which is thought to occur when a satellite’s halo is accreted into the larger halo of its host removing the satellite’s hot, diffuse gas and thus causing a slow decline (on timescales  $\tau > 1$  Gyr) in the star formation as its supply of cold gas is suppressed, and turning spirals into S0 galaxies. Kawata & Mulchaey (2008) simulate the strangulation process, showing that it acts on satellites within  $R < 500$  kpc on timescales of  $\tau \sim 2.0$  Gyr. They conclude the process is more effective in relaxed groups of galaxies, which are dominated by elliptical galaxies surrounded by an X-ray emitting intergalactic medium (IGM). Many of the systems with high mass hosts found in this study could be described as the system above, making strangulation a likely explanation for our results. This scenario is also consistent with the host mass having the largest effect on the red fraction, rather than satellite mass.

Compared to the slow quenching of star formation

which occurs in strangulation, rapid quenching could occur if enough external pressure is exerted on the satellite to remove its cold gas, in the process of ram pressure stripping (Gunn & Gott 1972; Hester 2006). Thought to turn spiral galaxies into S0 types, ram pressure stripping is most effective in clusters and groups of galaxies, where the density of the hot IGM and velocities of satellites creates sufficient pressure to overcome the restoring force keeping cold gas in galaxies. Hester (2006) finds, using simulations of groups, that low mass satellites are more severely stripped over larger distances, than larger spiral galaxies which are only stripped at small distances from the host. This is not what we see in this study with a higher red fraction over 0–0.4 Mpc, compared to the small neighbours, in the highest-mass hosts for all satellite masses [see Figure 8(e)].

Tidal stripping of gas from satellites due to the gravitational effects of the host is likely to occur simultaneously with ram-pressure stripping. Mayer et al. (2006), using N-body simulations of Milky Way sized halos surrounded by gas rich dwarfs, show that a combination of tidal and ram pressure stripping is more effective at removing gas than either process alone. Tidal interactions between satellites and their hosts may explain the streams of HI gas observed locally as the Magellanic Stream and High Velocity Clouds (Putman et al. 2003) and as the extragalactic HI clouds observed around M31 (Thilker et al. 2004), M33 (Grossi et al. 2008) and the M81/M82 group (Chynoweth et al. 2008). Shutting off of star formation might be expected to scale with the ratio of satellite to host mass, which is not evident in our data. Consider satellites that are  $\sim 0.01$ – $0.1$  times the mass of the host in Figure 8 [8.5–10 in Fig. 8(b), 9–10.5 in Fig. 8(d), 9.5–11 in Fig. 8(f)], it is clear that the difference between the satellites and small neighbours depends on the host mass but not the ratio between the satellite and host mass. This is in agreement with the idea that the probability of environment quenching is independent of the satellite stellar mass (Peng et al. 2011).

Another process which is thought to be able to strip galaxies of their gas is harassment (Moore et al. 1996). This is the heating of a satellite, occurring when a satellite’s DM sub-halo has frequent high-speed encounters with other DM sub-halos, turning low surface brightness discs into smaller dwarfs. Although this is usually considered as a process occurring in clusters containing thousands of galaxies,  $\Lambda$ CDM models of the Universe reveal that galaxy systems are scaled down versions of clusters and should contain thousands of dark matter sub-halos surrounding galaxies (Klypin et al. 1999; Moore et al. 1999), which means harassment on smaller scales may be a possibility.

Furthermore, satellite-satellite mergers could occur which would turn late-type satellites into early types (McIntosh et al. 2008). This however is unlikely to be a significant way of increasing the red fraction, due to the low numbers of satellites per host observed.

## 7 CONCLUSIONS

We have performed a search for the satellites of isolated galaxies from the GAMA survey using selection criteria that take into account stellar mass estimates. Separating galaxies into the red and blue populations using a colour-mass dia-

gram, we have investigated the radial distribution of satellites, and how the red fraction of satellites varies as function of projected distance, host stellar mass and satellite stellar mass.

We find out of a sample of 3514 isolated galaxies, 1426 which host a total of 2998 satellite galaxies. Separating the galaxies into red and populations, we find 41.2 per cent of the satellites are blue with red hosts, 33.3 per cent are red with red hosts, 22.2 per cent are blue with blue hosts and only 3.3 per cent are red with blue hosts. We find mean stellar masses and absolute magnitudes of  $\log_{10} \mathcal{M}_* = 10.00$  and  $M_r = -19.96$ , and  $\log_{10} \mathcal{M}_* = 9.35$  and  $M_r = -19.30$ , for the red and blue populations of satellites respectively. The average satellite in this sample is found to be  $\sim 1/10$ th of the mass of its host. The mean  $\Delta \log_{10} \mathcal{M}_* = 1.18$ . Our main results are as follows:

(i) Parametrizing the projected density of the satellites by  $\Sigma(R) \propto R^\alpha$ , we find best fitting slopes of  $\alpha \simeq -1.0$  for satellites divided into four host stellar mass bins (Fig. 5). By dividing the satellite hosts into red and blue populations we find the satellites of blue, low mass hosts to be more centrally concentrated. Power law slopes of  $\alpha = -0.94$  and  $\alpha = -1.05$  for the satellites of red and blue hosts are obtained, respectively. Correcting for interlopers the slopes steepen to  $\alpha = -1.13$  and  $\alpha = -1.38$  (Fig. 6).

(ii) We find there to be a steady increase in the red fraction of satellites as projected distance decreases for satellites with hosts of stellar mass  $\log_{10} \mathcal{M}_* \geq 10.5$ . The red fraction of satellites with hosts of stellar masses  $\log_{10} \mathcal{M}_* < 10.5$  shows no trend as a function of radius (Fig. 7).

(iii) Sub-dividing the satellite sample into host and satellite mass bins reveals that the host mass has the biggest effect on the satellite red fraction. Satellites with more massive hosts are more likely to be red. Comparing satellites to the small neighbours control sample, we find the red fraction is 0.13–0.25 higher for satellites of  $11.0 \leq \log_{10} \mathcal{M}_* \leq 11.5$  hosts, 0.06–0.15 higher for  $10.5 \leq \log_{10} \mathcal{M}_* \leq 11.0$  hosts, and almost unchanged for lower-mass  $10.0 \leq \log_{10} \mathcal{M}_* \leq 10.5$  hosts (Fig. 8).

The effect of environment, as noted by the difference between the satellites and small neighbours, can act over large range in high mass haloes and appears to be primarily a function of host mass and not satellite mass. These results suggest that quenching of star formation by strangulation is likely to be the main gas removal process in satellite systems, with other tidal effects, having a smaller contributing effect. Further study of the radial dependence of the instantaneous star formation rates of satellite galaxies using H $\alpha$  emission line measurements, is likely to yield more details about the quenching mechanism.

## ACKNOWLEDGEMENTS

GAMA is a joint European-Australasian project based around a spectroscopic campaign using the Anglo-Australian Telescope. The GAMA input catalogue is based on data taken from the Sloan Digital Sky Survey and the UKIRT Infrared Deep Sky Survey. Complementary imaging of the GAMA regions is being obtained by a number of independent survey programs including GALEX MIS, VST

KIDS, VISTA VIKING, WISE, Herschel-ATLAS, GMRT and ASKAP providing UV to radio coverage. GAMA is funded by the STFC (UK), the ARC (Australia), the AAO, and the participating institutions. The GAMA website is <http://www.gama-survey.org/>. MP acknowledges STFC for a postgraduate studentship. IKB and PAJ acknowledge STFC for funding. We acknowledge the IDL Astronomy User's Library, and IDL code maintained by D. Schlegel (IDLUTILS) as valuable resources.

We thank the anonymous referee for useful comments which have improved the content, clarity and presentation of this paper.

## REFERENCES

- Adelman-McCarthy J. K., et al., 2008, *ApJS*, 175, 297  
 Agustsson I., Brainerd T. G., 2010, *ApJ*, 709, 1321  
 Ann H. B., Park C., Choi Y., 2008, *MNRAS*, 389, 86  
 Azzaro M., Patiri S. G., Prada F., Zentner A. R., 2007, *MNRAS*, 376, L43  
 Bailin J., Power C., Norberg P., Zaritsky D., Gibson B. K., 2008, *MNRAS*, 390, 1133  
 Baldry I. K., Balogh M. L., Bower R. G., Glazebrook K., Nichol R. C., Bamford S. P., Budavari T., 2006, *MNRAS*, 373, 469  
 Baldry I. K., et al., 2010, *MNRAS*, 404, 86  
 Baldry I. K., Glazebrook K., Brinkmann J., Ivezić Ž., Lup-ton R. H., Nichol R. C., Szalay A. S., 2004, *ApJ*, 600, 681  
 Baldry I. K., Glazebrook K., Driver S. P., 2008, *MNRAS*, 388, 945  
 Balogh M. L., Navarro J. F., Morris S. L., 2000, *ApJ*, 540, 113  
 Bartelmann M., 1996, *A&A*, 313, 697  
 Bell E. F., et al., 2004, *ApJ*, 608, 752  
 Bell E. F., McIntosh D. H., Katz N., Weinberg M. D., 2003, *ApJS*, 149, 289  
 Bertin E., Arnouts S., 1996, *A&A*, 117, 393  
 Blanton M. R., Roweis S., 2007, *AJ*, 133, 734  
 Bower R. G., Benson A. J., Malbon R., Helly J. C., Frenk C. S., Baugh C. M., Cole S., Lacey C. G., 2006, *MNRAS*, 370, 645  
 Boylan-Kolchin M., Springel V., White S. D. M., Jenkins A., 2010, *MNRAS*, 406, 896  
 Brainerd T. G., 2005, *ApJ*, 628, L101  
 Busha M. T., Wechsler R. H., Behroozi P. S., Gerke B. F., Klypin A. A., Primack J. R., 2010, *ApJ*, submitted (arXiv:1011.6373)  
 Cameron E., 2010, *Publ. Astron. Soc. Australia*, in press (arXiv:1012.0566)  
 Chen J., 2008, *A&A*, 484, 347  
 Chen J., Kravtsov A. V., Prada F., Sheldon E. S., Klypin A. A., Blanton M. R., Brinkmann J., Thakar A. R., 2006, *ApJ*, 647, 86  
 Chynoweth K. M., Langston G. I., Yun M. S., Lockman F. J., Rubin K. H. R., Scoles S. A., 2008, *AJ*, 135, 1983  
 Colless M., et al., 2001, *MNRAS*, 328, 1039  
 Croton D. J., et al., 2006, *MNRAS*, 365, 11  
 Davis M., et al., 2003, *Proc. SPIE*, 4834, 161  
 De Propris R., Liske J., Driver S. P., Allen P. D., Cross N. J. G., 2005, *AJ*, 130, 1516  
 Domínguez-Palmero L., Balcells M., 2008, *A&A*, 489, 1003  
 Driver S. P., et al., 2009, *Astron. Geophys.*, 50, 5.12  
 Driver S. P., et al., 2011, *MNRAS*, 413, 971  
 Eke V. R., Baugh C. M., Cole S., Frenk C. S., Navarro J. F., 2006, *MNRAS*, 370, 1147  
 Faber S. M., et al., 2007, *ApJ*, 665, 265  
 Gallazzi A., Bell E. F., 2009, *ApJS*, 185, 253  
 Grossi M., Giovanardi C., Corbelli E., Giovanelli R., Haynes M. P., Martin A. M., Saintonge A., Dowell J. D., 2008, *A&A*, 487, 161  
 Gunn J. E., et al., 1998, *AJ*, 116, 3040  
 Gunn J. E., Gott III J. R., 1972, *ApJ*, 176, 1  
 Hau G. K. T., Bower R. G., Kilborn V., Forbes D. A., Balogh M. L., Oosterloo T., 2008, *MNRAS*, 385, 1965  
 Hester J. A., 2006, *ApJ*, 647, 910  
 Hill D. T., et al., 2011, *MNRAS*, 412, 765  
 Hogg D. W., Finkbeiner D. P., Schlegel D. J., Gunn J. E., 2001, *AJ*, 122, 2129  
 Hopkins P. F., Hernquist L., Cox T. J., Kereš D., 2008a, *ApJS*, 175, 356  
 Hopkins P. F., Hernquist L., Cox T. J., Younger J. D., Besla G., 2008b, *ApJ*, 688, 757  
 James P. A., Ivory C. F., 2011, *MNRAS*, 411, 495  
 Jones D. H., Saunders W., Colless M., Read M. A., Parker Q. A., Watson F. G., Campbell L. A., Burkey D., et al., 2004, *MNRAS*, 355, 747  
 Kawata D., Mulchaey J. S., 2008, *ApJ*, 672, L103  
 Klypin A., Kravtsov A. V., Valenzuela O., Prada F., 1999, *ApJ*, 522, 82  
 Lake G., Tremaine S., 1980, *ApJ*, 238, L13  
 Larson R. B., Tinsley B. M., Caldwell C. N., 1980, *ApJ*, 237, 692  
 Lawrence A., et al., 2007, *MNRAS*, 379, 1599  
 Le Fèvre O., et al., 2005, *A&A*, 439, 845  
 Liu L., Gerke B. F., Wechsler R. H., Behroozi P. S., Busha M. T., 2011, *ApJ*, 733, 62  
 Lorrimer S. J., Frenk C. S., Smith R. M., White S. D. M., Zaritsky D., 1994, *MNRAS*, 269, 696  
 Madore B. F., Freedman W. L., Bothun G. D., 2004, *ApJ*, 607, 810  
 Masters K. L., Haynes M. P., Giovanelli R., 2004, *ApJ*, 607, L115  
 Mayer L., Mastropietro C., Wadsley J., Stadel J., Moore B., 2006, *MNRAS*, 369, 1021  
 McIntosh D. H., Guo Y., Hertzberg J., Katz N., Mo H. J., van den Bosch F. C., Yang X., 2008, *MNRAS*, 388, 1537  
 Moore B., Ghigna S., Governato F., Lake G., Quinn T., Stadel J., Tozzi P., 1999, *ApJ*, 524, L19  
 Moore B., Katz N., Lake G., Dressler A., Oemler A., 1996, *Nature*, 379, 613  
 Navarro J. F., Frenk C. S., White S. D. M., 1996, *ApJ*, 462, 563  
 Peng Y., Lilly S. J., Renzini A., Carollo M., 2011, *ApJ*, submitted (arXiv:1106.2546)  
 Peng Y.-j., et al., 2010, *ApJ*, 721, 193  
 Petrosian V., 1976, *ApJ*, 209, L1  
 Phillipps S., Shanks T., 1987, *MNRAS*, 229, 621  
 Prescott M., Baldry I. K., James P. A., 2009, *MNRAS*, 397, 90  
 Putman M. E., Staveley-Smith L., Freeman K. C., Gibson B. K., Barnes D. G., 2003, *ApJ*, 586, 170

- Quinn P. J., Hernquist L., Fullagar D. P., 1993, *ApJ*, 403, 74
- Robotham A., et al., 2010, *Publ. Astron. Soc. Australia*, 27, 76
- Sales L., Lambas D. G., 2004, *MNRAS*, 348, 1236
- Sales L., Lambas D. G., 2005, *MNRAS*, 356, 1045
- Sales L. V., Navarro J. F., Lambas D. G., White S. D. M., Croton D. J., 2007, *MNRAS*, 382, 1901
- Schlegel D. J., Finkbeiner D. P., Davis M., 1998, *ApJ*, 500, 525
- Schmidt M., 1968, *ApJ*, 151, 393
- Sharp R., et al., 2006, *Proc. SPIE*, 6269, 62690G
- Smith R. M., Martínez V. J., Graham M. J., 2004, *ApJ*, 617, 1017
- Stoughton C., Lupton R. H., Bernardi M., Blanton M. R., Burles S., Castander F. J., Connolly A. J., Eisenstein D. J., 2002, *AJ*, 123, 485
- Strateva I., et al., 2001, *AJ*, 122, 1861
- Strauss M. A., et al., 2002, *AJ*, 124, 1810
- Taylor E. N., et al., 2011, *MNRAS*, in press
- Taylor E. N., Franx M., Glazebrook K., Brinchmann J., van der Wel A., van Dokkum P. G., 2010, *ApJ*, 720, 723
- Thilker D. A., Braun R., Walterbos R. A. M., Corbelli E., Lockman F. J., Murphy E., Maddalena R., 2004, *ApJ*, 601, L39
- Tollerud E. J., Boylan-Kolchin M., Barton E. J., Bullock J. S., Trinh C. Q., 2011, *ApJ*, in press (arXiv:1103.1875)
- Tonry J. L., Blakeslee J. P., Ajhar E. A., Dressler A., 2000, *ApJ*, 530, 625
- Toomre A., Toomre J., 1972, *ApJ*, 178, 623
- Vader J. P., Sandage A., 1991, *ApJ*, 379, L1
- van den Bosch F. C., Aquino D., Yang X., Mo H. J., Pasquali A., McIntosh D. H., Weinmann S. M., Kang X., 2008, *MNRAS*, 387, 79
- van den Bosch F. C., Yang X., Mo H. J., Norberg P., 2005, *MNRAS*, 356, 1233
- Weinmann S. M., van den Bosch F. C., Yang X., Mo H. J., 2006, *MNRAS*, 366, 2
- White S. D. M., Frenk C. S., 1991, *ApJ*, 379, 52
- Willmer C. N. A., et al., 2006, *ApJ*, 647, 853
- Yang X., Mo H. J., van den Bosch F. C., Jing Y. P., 2005, *MNRAS*, 356, 1293
- Yang X., Mo H. J., van den Bosch F. C., Pasquali A., Li C., Barden M., 2007, *ApJ*, 671, 153
- Yang X., van den Bosch F. C., Mo H. J., Mao S., Kang X., Weinmann S. M., Guo Y., Jing Y. P., 2006, *MNRAS*, 369, 1293
- York D. G., et al., 2000, *AJ*, 120, 1579
- Zaritsky D., Smith R., Frenk C., White S. D. M., 1993, *ApJ*, 405, 464
- Zibetti S., Charlot S., Rix H., 2009, *MNRAS*, 400, 1181

This paper has been typeset from a  $\mathrm{T}_{\mathrm{E}}\mathrm{X}/\mathrm{L}^{\mathrm{A}}\mathrm{T}_{\mathrm{E}}\mathrm{X}$  file prepared by the author.